Synthesis of Unsupported Pt-based Electrocatalysts and Evaluation of Their Catalytic Activity for the Ethylene Glycol Oxidation Reaction

A.F. Chávez Villanueva[1], Adriana M. Ramirez[1], G. Vargas Gutiérrez[2], L.A. Torres[2] and F.J. Rodríguez Varela[2,*]

[1]Universidad de la Ciénega de Michoacán de Ocampo, Avenida Universidad 3000, Sahuayo, Michoacán, México, CP 59000.
[2]CINVESTAV Unidad Saltillo, Carr. Saltillo-Monterrey km. 13.5, Ramos Arizpe, Coahuila, CP 25900

Abstract: *In this work, unsupported Pt, Pt-Ru (1:1 wt. % Pt:Ru ratio) and Pt-CeO$_2$ (1:1 wt. % Pt:CeO$_2$ ratio) electrocatalysts were synthesized and evaluated as anodes for the ethylene glycol oxidation reaction (EGOR) in out in H$_2$SO$_4$ electrolyte. The nanomaterials were prepared by slowly dropping the precursors in a NaBH$_4$ solution, in a reduction process of 10 min. Analysis by XRD showed the formation of polycrystalline electrocatalysts, while the chemical composition characterization indicated a ratio between the different elements in the bimetallic materials close to the stoichiometric value. Selected area electron diffraction patterns evaluation carried out in the TEM apparatus helped in the identification of Pt (1 1 1) in the three anodes, Ru (1 0 0) in Pt-Ru, and CeO$_2$ (1 1 1) in Pt-CeO$_2$, confirming the formation of Ru and CeO$_2$ phases. The results from the electrochemical characterization by Linear Scan Voltammetry (LSV) showed that the Pt-Ru material possess a higher mass catalytic activity for the EGOR, followed Pt-CeO$_2$, compared to Pt-alone. The nano-sized Pt-Ru and Pt-CeO$_2$ anodes demonstrated a high electrochemical stability in accelerated potential cycling tests, with very low surface area losses in the hydrogen adsorption/desorption region after 500 polarization cycles. The results indicated that the bimetallic electrocatalysts are candidate anodes for Direct Ethylene Glycol Fuel Cells.*

Keywords: Pt-Ru, Pt-CeO$_2$, nano-sized electrocatalysts, ethylene glycol oxidation reaction, Direct Ethylene Glycol Fuel Cells.

1. INTRODUCTION

Nanostructured materials have shown excellent physicochemical and electrochemical properties as catalysts for numerous reactions. This has been the reason why researchers worldwide have demonstrated a great interest in studying materials with different chemical compositions, as well as several structure configurations, from alloys to bimetallics to novel core-shell electrocatalysts [1, 2]. However, even though a large number of systems are being investigated, it is necessary to synthesize and characterize nanomaterials with particular catalytic properties. For example, in the case of Direct Alcohol Fuel Cells, there is the need to develop anodes with high catalytic activity for the oxidation of the specific fuel being used in the cell [3-6].

The methanol oxidation reaction (MOR) has been largely studied and the majority of the reports indicate that Pt-Ru systems are the most active anodes for such reaction [7-9]. Similarly, Pt-Sn anodes have shown a higher catalytic activity for the ethanol oxidation reaction (EOR) than Pt-alone or other Pt-based alloys [10-12]. Ru and Sn play the same role in the alloys, i.e., both materials activate the water discharge reaction at lower potentials than Pt in order to produce oxygen-containing surface species, which react with the reaction intermediates at Pt-sites to form CO$_2$ (bifunctional mechanism) [2]. Also, Ru and Sn modify the chemical properties of Pt leading to a reduction in the bonding strength between Pt and CO, according to the ligand effect [2, 13]. Baranova *et al.* relate the catalytic activity of bimetallic anodes for the EOR to the presence of Pt with large particle size in bi-phase Pt/SnO$_x$ and alloyed PtSn electrocatalysts [2]. In their investigations of the EOR, Sun *et al.* report that -OH species are formed at non-alloyed Pt-SnO$_2$/C anodes at relatively low potentials through the bifunctional mechanism, oxidizing adsorbed poisonous intermediates and increasing the yield of acetic acid [14]. Meanwhile, the same authors indicate that highly alloyed Pt-Sn/C anodes activate the dehydrogenation of ethanol to acetaldehyde, promoting the entire activity for the EOR due to the electronic effect [14]. In a
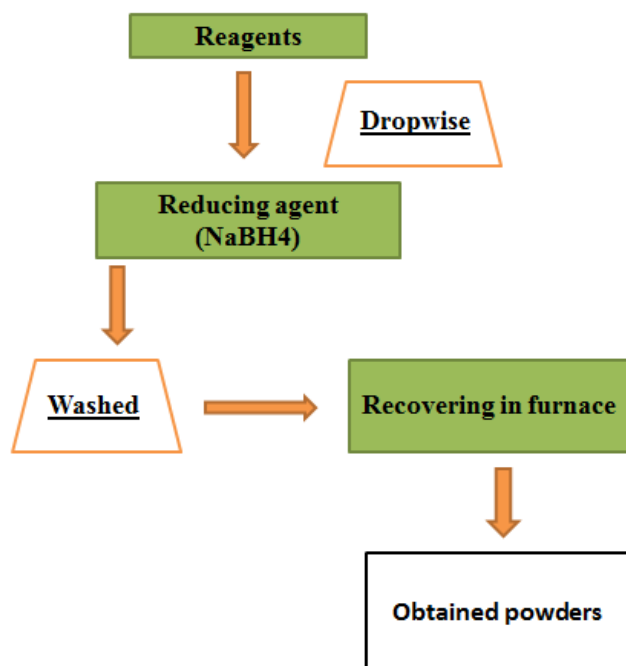
Figure 1. Schematic diagram showing the synthesis procedure to obtain the nanomaterials.

recent work, it has been shown that Ru@Pt core-shell nanostructures possess a higher catalytic activity for the EOR and the MOR than Pt-alone and the novel Fe_3O_4@Pt core-shell anode. Moreover, the novel Fe_3O_4@Pt showed also a higher catalytic activity for the EOR than Pt-alone, but a lower performance for the MOR [15]. The catalytic behavior of Fe_3O_4@Pt for the EOR and the MOR can be due to the different reaction intermediates formed from both anodic reactions, i.e., some of the intermediates produced during the MOR may have negatively affected the catalytic activity of Fe_3O_4@Pt and/or the capacity of Fe_3O_4 to act as an oxygen activator to form -OH surface species [15].

Besides methanol or ethanol, ethylene glycol (EG) has been studied as fuel for Direct Ethylene Glycol Fuel Cells (DEGFCs). In an electrochemical anodic reaction, EG delivers more electrons (10) than methanol (6): $C_2H_6O_2 + 2H_2O \rightarrow 2CO_2 + 10H^+ + 10e^-$. Moreover, EG has a higher theoretical capacity (4.8 vs. 4 Ah mL^{-1}) and is less dangerous in terms of toxicity and ecotoxicity than methanol [16, 17]. Several studies indicate that the electrocatalytic activity of Pt-Ru catalysts is higher than that of Pt-alone for the ethylene glycol oxidation reaction (EGOR) in acid media [18, 19]. There is also the interest to study other type of electrode compositions that have shown a high catalytic activity for the oxidation of organic molecules. This is the case of $Pt-CeO_2$ nanomaterials which have been reported as highly active for the oxidation of methanol and ethanol [20-26]. The role of CeO_2 in the $Pt-CeO_2$ system is the same as that of Ru and Sn in Pt-alloys, i.e., to activate the oxidation of organic molecules through the bi-functional mechanism [24].

In this work, alloyed Pt-Ru and bi-phase $Pt-CeO_2$ are evaluated as anodes for the oxidation of $C_2H_6O_2$ in acid media. For compari-

son, Pt-alone nanoparticles are also studied. The unsupported nanoparticles were synthesized by using sodium borohydride ($NaBH_4$) as reducing agent. The electrochemical performance of the nano-sized materials is evaluated by cyclic voltammetry (CV) and lineal scan voltammetry (LSV). The physicochemical characterization included XRD, TEM and EDS.

2. EXPERIMENTAL

2.1. Reagents and synthesis of nanomaterials

The reagents used to synthesize nanoparticles were of analytical grade and used without further treatment: $RuCl_3$ (Aldrich, 45.55% Ru), $H_2PtCl_6\times6H_2O$ (Aldrich, 37.5% Pt base), $CeN_3O_9\times6H_2O$ (Aldrich, 99%) as metallic precursors and $NaBH_4$ (Aldrich, 12% w/v in 14 M NaOH), as reducing agent. During the experimental procedure, Nafion (Alfa-Aesar, solution 5% w/w), H_2SO_4 (J.T. Baker, 98%), $C_2H_6O_2$ (Aldrich), N_2 and O_2 (UHP, Infra) were used.

The synthesis of nanomaterials was performed by slowly dropping the precursors in a $NaBH_4$ solution. The Pt-alone catalyst was obtained in a reduction process of 10 min. In the case of Pt-Ru and $Pt-CeO_2$, the Pt precursor was introduced first and submitted to reduction for 10 min, followed by the addition of the Ru or CeO_2 precursors, which were also reduced for 10 min. The recovered powders were washed with excess water and dried in a furnace at 80 °C. Figure 1 shows a schematic diagram of the synthesis procedure. The molar ratio used for obtaining the powders is shown in Table 1.

2.2. Physical and chemical characterization

The electrocatalysts were characterized in a Philips X´Pert XRD diffractometer using a Cu Ka radiation source ($\lambda K\alpha1 = 1.54060$ Å). Diffractograms were acquired over 10-100 degrees with 0.025 steps and the XRD patterns were identified with the JCPDS data base. TEM and EDS studies were carried out in a field emission gun microscope FEI-TITAN 80-300 kV, operated at 300 kV.

2.3. Electrode preparation and electrochemical setup

The catalyst ink of each nanocatalyst was prepared following a previously reported procedure [26, 27]. Each electrocatalyst powder was independently mixed by ultrasound to form a catalyst ink of 5 mg_{catal}/mL. An aliquot of 10 mL was pipetted onto a glassy carbon disc (geometric area of 0.196 cm^2, mirror polished with 0.05 mm alumina). Activation of the nanostructures was performed by cyclic voltammetry (CV) by taking potential cycles at 50 mV s^{-1} in N_2-saturated 0.5 M H_2SO_4 in 0.05 to 1.2 V potential intervals (vs. SHE), with a Voltalab potentiostat connected to a rotating disc setup (Pine Inst.). In this work, 40 cycles were sufficient to obtain

Table 1. Reagents concentration

Material	Reagent concentration (mol L^{-1})			$NaBH_4$ concentration (mol L^{-1})
	$H_2PtCl_6\times6H_2O$	$RuCl_3$	$CeN_3O_9\times6H_2O$	
Pt	0.000513			0.000075
Pt-Ru	0.001538	0.002950		0.001299
$Pt-CeO_2$	0.001538		0.002141	0.000599
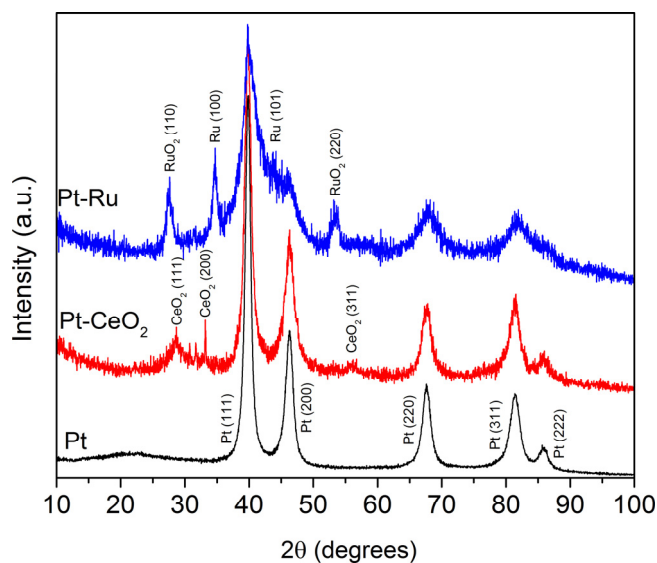
Figure 2. Diffraction patterns of the electrocatalysts.

Figure 3. TEM images of Pt (a, b), Pt-Ru (c, d) and Pt-CeO$_2$ (e, f).

reproducible voltammograms. After activation, CVs were acquired at the scan rate of 20 mV s^{-1}. Then, the catalytic activity for the EGOR of the nanomaterials was evaluated. CVs were collected in the anodic direction at the scan rate of 20 mV s^{-1} in the same potential interval, in a 0.5 M H$_2$SO$_4$ + 0.5 M C$_2$H$_6$O$_2$ solution. The electrochemical set-up included a Pt mesh as counter electrode, with an Ag/AgCl reference electrode, although all potentials are reported here against the Standard Hydrogen Electrode (SHE). All electrochemical experiments were performed at room temperature.

3. RESULTS AND DISCUSSION

3.1. Physicochemical characterization

Figure 2 shows the diffractograms of Pt, Pt-Ru and Pt-CeO$_2$. The Pt pattern depicts the (111), (200), (220), (311) and (222) reflections at about 2θ=39.9, 46.3, 67.6, 81.4 and 85.8 respectively, typical of polycrystalline fcc platinum structure. The Pt-CeO$_2$ pattern shows the Pt peaks and also shows the reflections that correspond to the (111), (200) and (311) CeO$_2$ planes at about 2θ=28.6, 39.7 and 56.7. Meanwhile, the diffractogram of Pt-Ru shows the presence of the Ru (100) and (101) planes at 2θ=34.6 and 43.6, as well those of RuO$_2$ (110) and (220) at 2θ=27.3 and 53.1, respectively.

Figure 3 shows the TEM images of the anodes. The nanoparticles tend to form agglomerates, while selected area electron diffraction (SAED) patterns indicate their crystalline features (see Figs. 3(a), (c) and (e), and the inserts therein). With the high resolution capability of the apparatus it is possible to observe lattice fringes of Pt in Fig. 3(b). Fourier analysis in the selected nanoparticle made possible to determine the distance d between adjacent planes. In this case, d=0.2252 nm, which is ascribed to the Pt (1 1 1) plane. The Fourier analysis of Pt-Ru in the square of Fig. 3(d) shows the presence of two interplanar distances, d=0.2192 nm that corresponds to Pt (1 1 1) and d=0.2560 attributed to Ru (1 0 0). The co-existence Pt and Ru suggests the formation of the Pt-Ru alloy. Finally, the HRTEM analysis of the Pt-CeO$_2$ material is shown in Fig. 3(f). It is possible to discern Pt from CeO$_2$ nanoparticles from
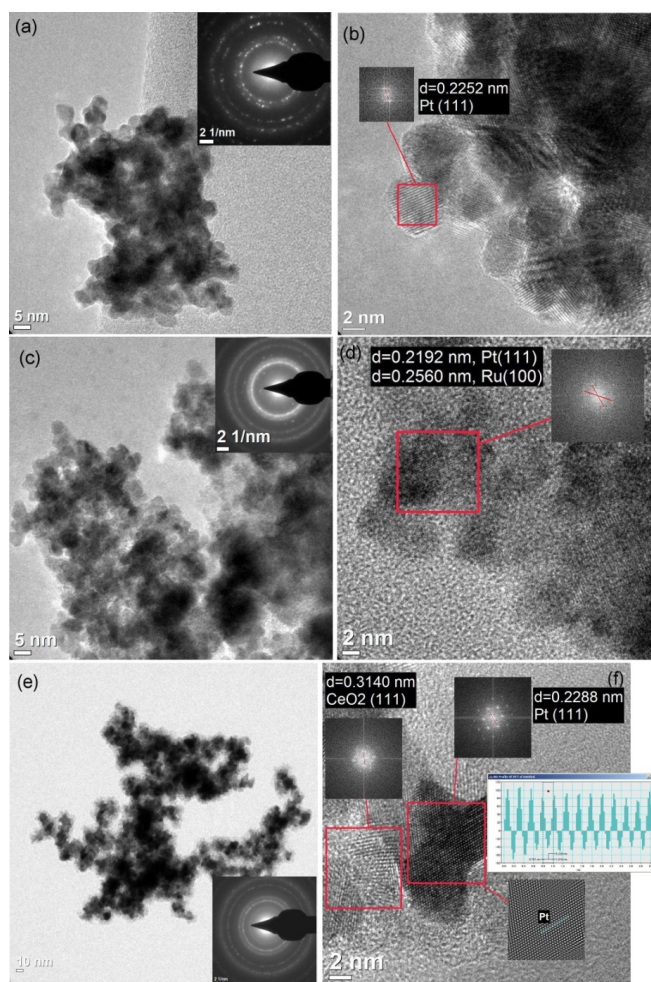
the contrast observed and the Fourier evaluation that shows a d value of 0.2288 nm in the darker zone, which is confirmed by the profile estimation in the same area (d=0.226 nm, see profile insert in Fig. 3f). Both analyses indicate that the interplanar distance in such zone corresponds to Pt (1 1 1). Meanwhile, the d value in the clearer area is 0.3140 nm, ascribed to the CeO$_2$ (1 1 1) plane.

The EDS results obtained in the TEM apparatus are shown in Table 2. As can be observed, the chemical composition of Pt:Ru is 54.52:45.47, nearly the nominal composition of 1:1 wt. % Pt:Ru ratio. Meanwhile, the chemical composition of Pt-CeO$_2$ differs from the nominal one, with a Pt:CeO$_2$ ratio of 1.5:1 wt. %. The presence of about 11.5 % O (wt. %) suggests the formation of CeO$_2$ in the Pt-CeO$_2$ material.

Table 2. Chemical composition of the nanostructured materials.

Catalyst	Pt (wt. %)	Ru (wt. %)	Ce (wt. %)	O (wt. %)
Pt	100	-	-	-
Pt-Ru	54.52	45.47	-	-
Pt-CeO$_2$	59.10		29.34	11.54
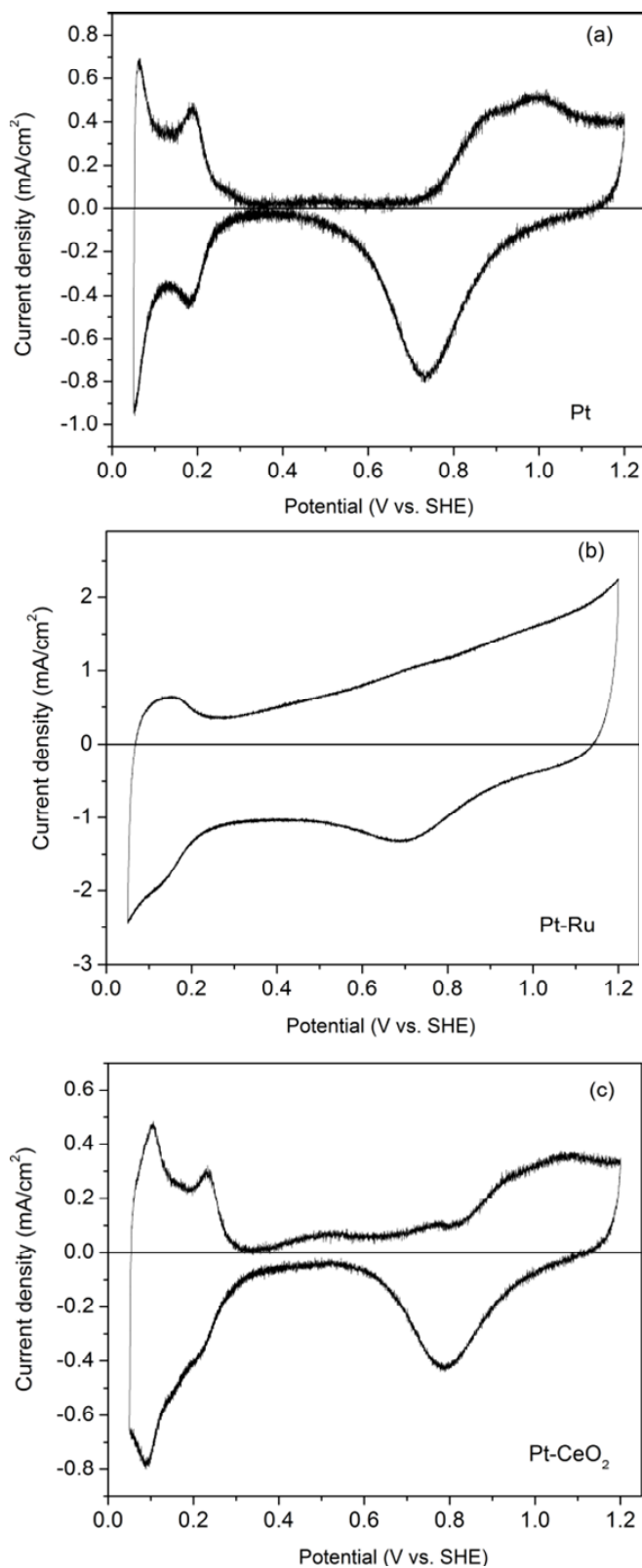
Figure 5. Mass catalytic activity of Pt, Pt-Ru and Pt-CeO$_2$ for the EGOR. Electrolyte: 0.5M H$_2$SO$_4$. Scan rate 20 mV s^{-1}.

Figure 4 shows the CVs of Pt, Pt-Ru and Pt-CeO$_2$. The CV of Pt (Fig. 4a) depicts the typical characteristics of this material: i) two well defined peaks due to the hydrogen adsorption/desorption process in the 0.05-0.25 V interval; ii) very low current densities in the double layer above 0.3 V; iii) a Pt-oxides region with two broad shoulders at around 0.88 and 0.98 V in the positive scan and a current density peak due to the oxides reduction at nearly 0.73 V in the negative scan. The Pt-Ru material (Fig. 4b) shows a less defined hydrogen region related to Pt-alone, a characteristic that may be attributed in part to the formation of a Pt-Ru alloy phase, because peaks related to the hydrogen adsorption/desorption are not clearly defined at Ru materials. Another characteristic of this alloy is that it shows a large double layer region and a less defined oxides region. Meanwhile, the Pt-CeO$_2$ material in Fig. 4(c) shows characteristics that overall resemble those of Pt-alone, although the presence of CeO$_2$ caused some changes. For example the H$_{ads}$ peaks are not so well defined and instead a large area emerged in the 0.25-0.05 mV interval (negative scan). Also, the double layer region in the positive scan shows a current slope and is not completely parallel to the zero current line. Moreover, although the Pt-oxides region at potentials above 0.85 V is slightly less defined than in the case of Pt-alone in Fig. 4(a), the oxides formation/reduction can be observed. These characteristics of the chemically synthesized anode differ from the results obtained previously at similar Pt-CeO$_2$ materials, where the presence of the cerium oxide suppressed the Pt-oxides formation/reduction and the hydrogen adsorption/desorption peaks are absent both in acid and alkaline medium [28, 29]. The Pt-like characteristics of the CV in Figure 4(c) may be attributed to several factors: i) the Pt precursor is reduced first for 10 min in NaBH$_4$, promoting the formation of metallic Pt; ii) the Pt nanoparticles may not be covered by a CeO$_2$ film during the reduction of the cerium precursor as described in ref. [30], but rather separated phases of Pt and CeO$_2$ may be formed, as can be observed from the TEM image in Fig. 3(f); ii) the Pt:CeO$_2$ wt. % ratio, which in this work is 1.5:1 (i.e., Pt-rich), contributes to the shape of the CV of Pt-CeO$_2$ in Fig. 4(c).

Figure 4. CVs of Pt-alone (a), Pt-Ru (b) and Pt-CeO$_2$ (c). Electrolyte: 0.5M H$_2$SO$_4$ saturated with N$_2$. Scan rate: 20 mV s^{-1}.
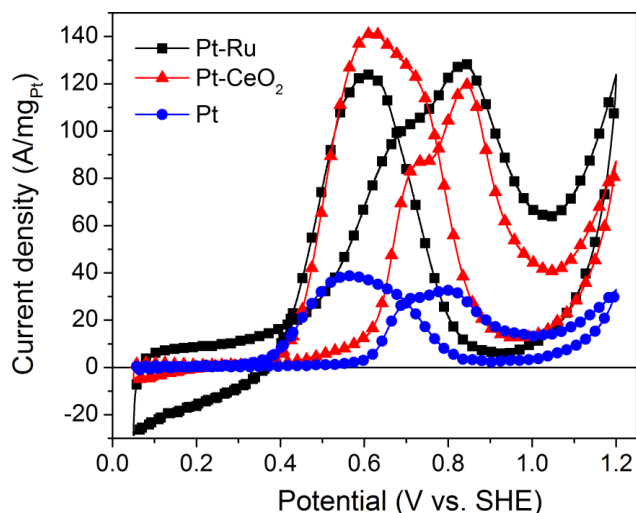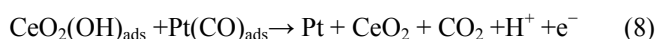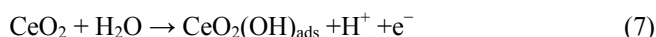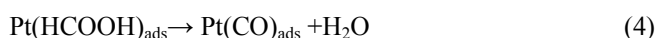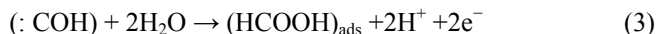
Figure 5 shows the mass catalytic activity for the EGOR (considering the amount of Pt at each anode) of Pt-alone, Pt-Ru and Pt-CeO$_2$. The reaction starts at lower potentials at Pt-Ru (onset potential about 0.25 V vs. SHE), followed by Pt-CeO$_2$ and Pt (onset potentials around 0.4 V and 0.58 V vs. SHE, respectively). In the positive scan, one shoulder emerges at 0.69 V and 0.71 V at Pt-Ru and Pt-CeO$_2$, respectively, while a maximum peak current density can be observed at about 0.83 V at both nanocatalysts. The appearance of two peaks due to the EGOR has been attributed to the partial oxidation of ethylene glycol to C$_2$ by-products and/or ethylene glycol dissociation to CO [31, 32]. The maximum current density at such potential is 127 and 119 A mg$_{Pt}^{-1}$ for Pt-Ru and Pt-CeO$_2$, respectively. Meanwhile, the catalytic activity of Pt-alone for the EGOR is significantly lower than the activity of the other two anodes. It can be noticed that the ratio between the forward and backward sweeps is lower in the case of Pt-CeO$_2$ compared to Pt-Ru, suggesting a stronger poisoning of the cerium-containing anode due to the reaction intermediates produced during the EGOR [12].

The enhanced catalytic activity of Pt-Ru and Pt-CeO$_2$ related to Pt can be attributed to the bi-functional mechanism, i.e., the promotion of CO$_{ads}$ to CO$_2$ by the participation of Ru or CeO$_2$ in the water discharge reaction to form oxygenated species at lower potentials than Pt-alone [5]. The EG oxidation mechanism has been proposed before [5, 19]. For example, in the case of CeO$_2$ can be written in a similar fashion as that of Ru [5]:

$$(CH_2OH)_2 \rightarrow (CH_2OH)_{2(ads)} \qquad (1)$$

$$(CH_2OH)_{2(ads)} \rightarrow (: COH)_2 \qquad (2)$$

$$(: COH) + 2H_2O \rightarrow (HCOOH)_{ads} + 2H^+ + 2e^- \qquad (3)$$

$$Pt(HCOOH)_{ads} \rightarrow Pt(CO)_{ads} + H_2O \qquad (4)$$

$$Pt + H_2O \rightarrow Pt(OH)_{ads} \qquad (5)$$

$$Pt(OH)_{ads} + Pt(CO)_{ads} \rightarrow Pt + CO_2 + H^+ \qquad (6)$$

$$CeO_2 + H_2O \rightarrow CeO_2(OH)_{ads} + H^+ + e^- \qquad (7)$$

$$CeO_2(OH)_{ads} + Pt(CO)_{ads} \rightarrow Pt + CeO_2 + CO_2 + H^+ + e^- \qquad (8)$$

Besides the evaluation of the catalytic activity of Pt-Ru and Pt-CeO$_2$ for the EGOR, it is important to study the electrochemical durability of the nanostructures [26]. The process is as follows: after activation of the catalysts and the acquisition of CVs at 20 mV s^{-1} between 0.05 and 1.2 V vs. SHE (i.e., those shown in Fig. 4), the working electrode is subjected to 500 potential cycling at 0.6 and 1.2 V vs. SHE, emulating high fuel cell operating potentials and strongly oxidizing conditions. Then, another set of CVs at 20 mV s^{-1} is obtained between 0.05 and 1.2 V vs. SHE. Afterwards, the losses in surface area can be evaluated by comparing the characteristics of the CVs taken before and after potential polarization.

Figure 6 shows the CVs of Pt-Ru and Pt-CeO$_2$ in N$_2$-saturated solution before and after potential cycles. It can be observed that the surface area reduction in the hydrogen adsorption-desorption region is not significant. For example, there is less than 15 % loss after cycling, related to the surface area before the polarization test at Pt-Ru. From the results in this Figure, it can be concluded that the Pt-Ru and Pt-CeO$_2$ systems show a high stability in H$_2$SO$_4$.
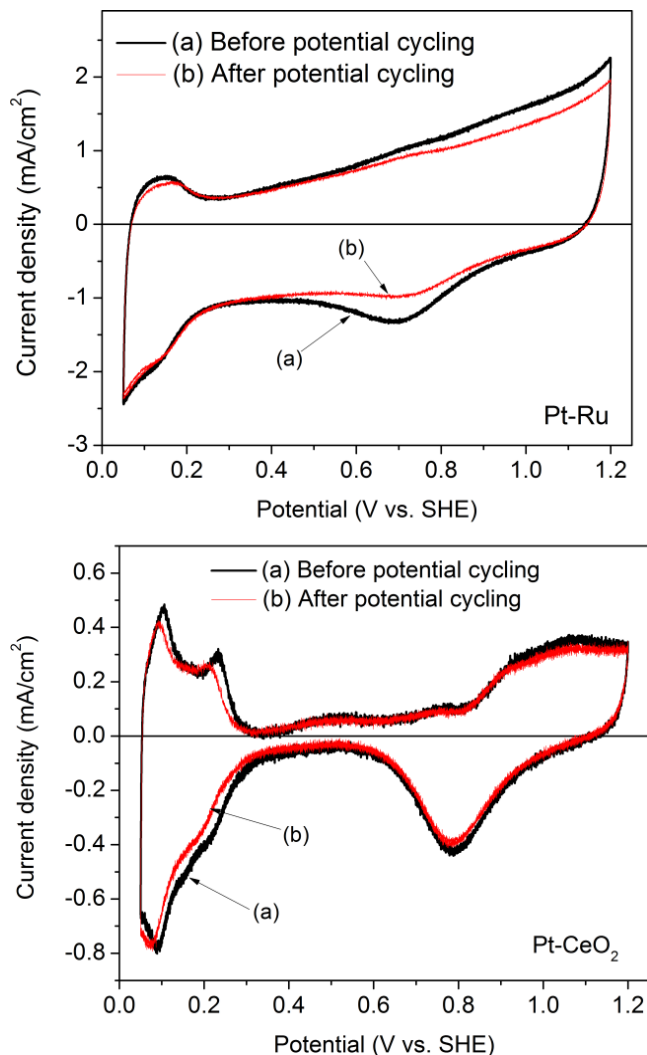

Figure 6. CVs of the Pt-Ru and Pt-CeO$_2$ systems acquired at the scan rate of 20 mV s^{-1}, before and after 500 polarization cycles between 0.6 and 1.2 V vs. SHE at 50 mV s^{-1}.

4. CONCLUSIONS

The nanoparticles synthesized in NaBH$_4$ solution showed polycrystalline features. The TEM analysis indicated the formation of nanostructured materials while Fourier analysis in selected areas made possible to determine the distance between adjacent planes. In the case of Pt-alone, the Pt (1 1 1) plane was indentified. Meanwhile, for Pt-Ru and Pt-CeO$_2$, besides Pt (1 1 1), it was possible to ascribe lattice fringes to Ru (1 0 0) and CeO$_2$ (1 1 1) planes, respectively. The chemical composition analyses confirmed the formation of Pt-Ru with 1:1 Pt:Ru ratio (wt. %), in good agreement with nominal calculations. Meanwhile, the Pt-CeO$_2$ was formed with a 1.5:1 Pt:CeO$_2$ ratio (wt. %), indicating a larger amount of Pt than predicted. The electrocatalytic activity of the nanostructured catalysts for the EGOR was evaluated in acid medium. The mass catalytic activity of the Pt-Ru and Pt-CeO$_2$ anodes was significantly higher than that of Pt-alone. Such enhanced catalytic activity has

been attributed to the bi-functional mechanism. Moreover, the nano-sized Pt-Ru and Pt-CeO$_2$ anodes demonstrated a high electrochemical stability in accelerated potential cycling tests, with very low surface area losses in the hydrogen adsorption/desorption region after 500 polarization cycles between 0.6 and 1.2 V vs. SHE.

5. AKCNOWLEDGEMENTS

REFERENCES

[1] S. Alayoglu, A.U. Nilekar, M. Mavrikakis, B. Eichhorn, Nature Materials, 7, 333 (2008).

[2] E.A. Baranova, T. Amir, P.H.J. Mercier, B. Patarachao, D. Wang, Y. Le Page, J. Appl. Electrochem., 40, 1767 (2010).

[3] E. Antolini, J. Power Sources, 170, 1 (2007).

[4] E. Antolini, E.R. Gonzalez, J. Power Sources, 195, 3431 (2010).

[5] A. Serov, C. Kwak, Appl. Catal. B: Environ., 97, 1 (2010).

[6] K. Matsuoka, Y. Iriyama, T. Abe, M. Matsuoka, Z. Ogumi, J. Power Sources, 150, 27 (2005)

[7] A.S. Aricòa, S. Srinivasan, V. Antonucci, Fuel Cells, 1, 133 (2001).

[8] W.H. Lizcano-Valbuena, A. de Souza, V.A. Paganin, C.A.P. Leite, F. Galembeck, E.R. Gonzalez, Fuel Cells, 2, 159 (2002).

[9] M. Neergat, D. Leveratto, U. Stimming, Fuel Cells, 2, 25 (2002).

[10] F. Vigier, C. Coutanceau, A. Perrard, E.M. Belgsir, C. Lamy, J. Appl. Electrochem., 34, 439, (2004).

[11] C. Lamy, S. Rousseau, E.M. Belgsir, C. Coutanceau, J.-M. Léger, Electrochim. Acta, 49, 3901 (2004).

[12] C. Lamy, E.M. Belgsir, J.-M. Léger, J. Appl. Electrochem., 31, 799, (2001).

[13] P.E. Tsiakaras, J. Power Sources, 171, 102 (2007).

[14] M. Zhu, G. Sun, Q. Xin, Electrochim. Acta, 54, 1511 (2009).

[15] N.M. Sánchez-Padilla, S.M. Montemayor, L.A. Torres, F.J. Rodríguez Varela, Int. J. Hydrogen Energy, DOI: 10.1016/j.ijhydene.2012.11.026.

[16] V. Livshits, A. Philosoph, E. Peled, J. Power Sources, 178, 687 (2008).

[17] U.B. Demirci, Environ. Int., 35, 626 (2009).

[18] R.B. De Lima, V. Paganin, T. Iwasita, W. Vielstich, Electrochim. Acta, 49, 85 (2003).

[19] V. Selvaraj, M. Vinoba, M. Alagar, J. Colloid Interface Sci., 322, 537 (2008).

[20] Y. Zhao, F. Wang, J. Tian, X. Yang, Lu Zhan, Electrochim. Acta, 55, 8998 (2010).

[21] M.A. Scibioh, S.-K. Kim, E.A. Cho, T.-H. Lim, S.-A. Hong, H.Y. Ha, Appl. Catal. B: Environm., 84, 773 (2008).

[22] Y. Zhou, Y. Gao, Y. Liu, J. Liu, J. Power Sources, 195, 1605 (2010).

[23] D.-J. Guo, Z.-H. Jing, J. Power Sources, 195, 3802 (2010).

[24] R.F.B. De Souza, A.E.A. Flausino, D.C. Rascio, R.T.S. Oliveira, E. Teixeira Neto, M.L. Calegaro, M.C. Santos, Appl. Catal. B: Environm., 91, 516 (2009).

[25] J. Wang, J. Xi, Y. Bai, Y. Shen, J. Sun, L. Chen, W. Zhu, X. Qiu, J. Power Sources, 164, 555 (2007).

[26] Nora Mayté Sánchez-Padilla, Sagrario M. Montemayor, F.J. Rodríguez Varela, J. New Mat. Electrochem. Systems, 15, 171 (2012).

[27] F.J. Rodriguez Varela, A.A. Gaona Coronado, J.C. Loyola, Qi-Zhong Jiang, P. Bartolo Perez, J. New Mat. Electrochem. Systems, 14, 75 (2011).

[28] T. Masuda, H. Fukumitsu, K. Fugane, H. Togasaki, D. Matsumura, K. Tamura, Y. Nishihata, H. Yoshikawa, K. Kobayashi, T. Mori, K. Uosaki K, J. Phys. Chem. C, 116, 10098 (2012).

[29] A. Altamirano-Gutiérrez, A.M. Fernández, F.J. Rodríguez Varela, Int. J. Hydrogen Energy, DOI: http://dx.doi.org/10.1016/j.ijhydene.2012.12.140.

[30] K. Fugane, T. Mori, D.R. Ou, A. Suzuki, H. Yoshikawa, T. Masuda, K. Uosaki, Y. Yamashita, S. Ueda, K. Kobayashi, N. Okazaki, I. Matolinova and V. Matolin, Electrochim. Acta, 56, 3874 (2011).

[31] V. Livshits and E. Peled, J. Power Sources, 161, 1187 (2006).

[32] R. Chetty and K. Scott, J. Appl. Electrochem., 37, 1077 (2007).